Inorg. Chem. **2008**, *47*, 8222−8232

Reactions of Copper(II)-H_2O_2 Adducts Supported by Tridentate Bis(2-pyridylmethyl)amine Ligands: Sensitivity to Solvent and Variations in Ligand Substitution

Atsushi Kunishita,[†] Joseph D. Scanlon,[‡] Hirohito Ishimaru,[§] Kaoru Honda,[||] Takashi Ogura,[§] Masatatsu Suzuki, Christopher J. Cramer,[*,‡] and Shinobu Itoh[*,†]

Department of Chemistry, Graduate School of Science, Osaka City University, 3-3-138 Sugimoto, Sumiyoshi-ku, Osaka 558-8585, Japan, Department of Chemistry and Research Computing Center, University of Minnesota, 207 Pleasant Street SE, Minneapolis, Minnesota 55455, Graduate School of Life Science, University of Hyogo, 3-2-1 Kouto, Kamigori-cho, Ako-gun, Hyogo 678-1297, Japan, and Division of Material Sciences, Graduate School of Natural Science and Technology, Kanazawa University, Kakuma-machi, Kanazawa, 920-1192, Japan

Received May 9, 2008

The copper(II) complexes $\mathbf{1^H}$ and $\mathbf{1^{Ar(X)}}$, supported by the *N,N*-di(2-pyridylmethyl)benzylamine tridentate ligand (L^H) or its derivatives having *m*-substituted phenyl group at the 6-position of pyridine donor groups ($L^{Ar(X)}$), have been prepared, and their reactivity toward H_2O_2 has been examined in detail at low temperature. Both copper(II) complexes exhibited a novel reactivity in acetone, giving 2-hydroxy-2-hydroperoxypropane (HHPP) adducts $\mathbf{2^H}$ and $\mathbf{2^{Ar(X)}}$, respectively. From $\mathbf{2^{Ar(X)}}$, an efficient aromatic ligand hydroxylation took place to give phenolate-copper(II) complexes $\mathbf{4^{Ar(X)}}$. Detailed spectroscopic and kinetic analyses have revealed that the reaction proceeds via an electrophilic aromatic substitution mechanism involving copper(II)-carbocation intermediates $\mathbf{3^{Ar(X)}}$. Theoretical studies at the density functional theory (DFT) level have strongly implicated conjugate acid/base catalysis in the O−O bond cleavage and C−O bond formation steps that take the peroxo intermediate $\mathbf{2^{Ar(X)}}$ to the carbocation intermediate $\mathbf{3^{Ar(X)}}$. In contrast to the $\mathbf{2^{Ar(X)}}$ cases, the HHPP-adduct $\mathbf{2^H}$ reacted to give a copper(II)-acetate complex $[Cu^{II}(L^H)(OAc)](ClO_4)$ ($\mathbf{6^H}$), in which one of the oxygen atoms of the acetate co-ligand originated from H_2O_2. In this case, a mechanism involving a Baeyer−Villiger type 1,2-methyl shift from the HHPP-adduct and subsequent ester hydrolysis has been proposed on the basis of DFT calculations; conjugate acid/base catalysis is implicated in the 1,2-methyl shift process as well. In propionitrile, both $\mathbf{1^H}$ and $\mathbf{1^{Ar(X)}}$ afforded simple copper(II)-hydroperoxo complexes LCu^{II}−OOH in the reaction with H_2O_2, demonstrating the significant solvent effect on the reaction between copper(II) complexes and H_2O_2.

Introduction

The reactions of copper(II) complexes and hydrogen peroxide (H_2O_2) have been studied extensively to gain insight into the structure, physicochemical properties, and reactivity of the various reactive intermediates involved in copper monooxygenases and copper oxidases, as well as numerous copper catalyzed oxidation reactions.[1−5] In many cases, the reaction yields a mononuclear copper(II)-hydroperoxo complex LCu^{II}−OOH (**A** in Chart 1), exhibiting an intense absorption band around 325−387 nm assigned to a $HOO^-\rightarrow Cu^{II}$ ligand-to-metal charge transfer (LMCT) transi-

* To whom correspondence should be addressed. E-mail: shinobu@sci.osaka-cu.ac.jp (S.I.), cramer@umn.edu (C.J.C.).
[†] Osaka City University.
[‡] University of Minnesota.
[§] University of Hyogo.
[||] Kanazawa University.

(1) (a) Wada, A.; Harata, M.; Hasegawa, K.; Jitsukawa, K.; Masuda, H.; Mukai, M.; Kitagawa, T.; Einaga, H. *Angew. Chem., Int. Ed.* **1998**, *37*, 798–799. (b) Yamaguchi, S.; Wada, A.; Nagatomo, S.; Kitagawa, T.; Jitsukawa, K.; Masuda, H. *Chem. Lett.* **2004**, 1556–1557. (c) Mizuno, M.; Honda, K.; Cho, J.; Furutachi, H.; Tosha, T.; Matsumoto, T.; Fujinami, S.; Kitagawa, T.; Suzuki, M. *Angew. Chem., Int. Ed.* **2006**, *45*, 6911–6914. (d) Maiti, D.; Sarjeant, A. A. N.; Karlin, K. D. *J. Am. Chem. Soc.* **2007**, *129*, 6720–6721. (e) Maiti, D.; Lucas, H. R.; Sarjeant, A. A. N.; Karlin, K. D. *J. Am. Chem. Soc.* **2007**, *129*, 6998–6999.

10.1021/ic800845h CCC: $40.75
Published on Web 08/13/2008

Chart 1

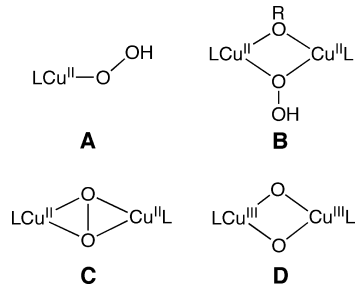

tion and a resonance Raman band at 822−900 cm^{-1} attributable to the O−O bond stretching vibration of the −OOH group.[1−3] The mononuclear copper(II)-hydroperoxo complex **A** has been suggested as one of the important intermediates involved in the copper monooxygenases such as peptidylglycine α-amidating monooxygense (PAM) and dopamine β-monooxygenase (DβM), as well as in copper oxidases such as copper-containing amine oxidases (AO) and galactose oxidase (GAO).[6]

In some cases, the reactions of copper(II) complexes with H_2O_2 have given dinuclear copper(II) complexes **B** (R = Ar or H) containing a μ-η^1:η^1-hydroperoxo bridge; these exhibit similar spectroscopic features to those of complex **A**.[4] The (μ-η^2:η^2-peroxo)dicopper(II) and bis(μ-oxo)dicopper(III) complexes, **C** and **D**, have also been generated in rare cases.[5] The physicochemical properties and reactivity of such dinuclear copper complexes have been studied extensively to shed light on the mechanistic details of copper proteins (enzymes) incorporating a dinuclear copper moiety in their active sites such as hemocyanin (dioxygen carrier protein), catechol oxidase, and tyrosinase (monooxygenase), although compounds **C** and **D** are more typically generated by the reaction of copper(I) complexes with molecular oxygen.[7,8]

For the preparation of mononuclear copper(II)-hydroperoxo complex **A**, *tetradentate* tripodal ligands such as tris(2-pyridylmethyl)amine (TPA) and its derivatives have been frequently employed. In this ligand system, metastable end-on hydroperoxo complexes with a trigonal bipyramidal geometry are obtained, since such tetradentate ligands afford only one vacant coordination site for the external ligands.[1] The most prominent example is the first X-ray structure determination of LCu^{II}−OOH (**A**) by Masuda and co-workers using a TPA derivative involving two 6-pivalamide-2-pyridylmethyl groups.[1a] In this complex, the end-on hydroperoxo complex is further stabilized by an intramolecular hydrogen bonding interaction between the pivalamide NH groups and the proximal oxygen atom of the −OOH group.[1a] Likely because of this, Masuda's hydroperoxo complex exhibits little redox reactivity.[9]

With respect to the oxygenation reactivity of copper(II)−H_2O_2 adducts, Karlin and co-workers recently reported oxidative *N*-dealkylation and aromatic hydroxylation reactions when supported copper(II) complexes were treated with H_2O_2 in acetone in the presence of triethylamine as a base.[1d,e] In these cases, a dimethylamino group (−NMe_2) or a *p-tert*-butylphenyl group (−C_6H_4-*p*-^{t}Bu), respectively, was attached at the 6-position of one of the pyridine rings of TPA.[1d,e] The authors suggested that a LCu^{II}−OOH intermediate (**A**) was the reactive species in both reactions.[1d,e] By contrast, Suzuki and co-workers reported an auto-oxidation type ligand modification (formation of a ligand-based alkylperoxo-copper(II) complex) from the reaction of H_2O_2 and a copper(I) complex supported by bis(6-methyl-2-pyridylmethyl)(2-pyridylmethyl)amine (Me_2-TPA) in acetonitrile.[1c] They suggested that a Cu(III)═O type species (also formulated as Cu(II)−$O^{\bullet-}$) was a possible active intermediate for the hydrogen atom abstraction from the 6-methyl group of ligand that was inferred as the initial step of the auto-oxidation type chain reaction.[1c]

Recently, we have found that copper(II) complexes supported by *tridentate* bis(2-pyridylmethyl)amine ligands containing a series of *m*-substituted phenyl groups at the 6-position of pyridines ($L^{Ar(X)}$, X = OMe, Me, H, Cl, and NO_2, see Chart 2), when treated with H_2O_2 in *acetone* in the presence of triethylamine (i.e., nearly the same experimental conditions as those for Karlin's reactions mentioned above), gave a new type of Cu^{II}−H_2O_2 adduct **E** (Scheme 1).[10] In our case, an acetone molecule is incorporated into the complex to make a 2-hydroxy-2-hydroperoxypropane (HHPP) adduct, which then undergoes an efficient aromatic ligand

(2) (a) Ohtsu, H.; Itoh, S.; Nagatomo, S.; Kitagawa, T.; Ogo, S.; Watanabe, Y.; Fukuzumi, S. *Chem. Commun.* **2000**, 1051–1052. (b) Kodera, M.; Kita, T.; Miura, I.; Nakayama, N.; Kawata, T.; Kano, K.; Hirota, S. *J. Am. Chem. Soc.* **2001**, *123*, 7715–7716. (c) Ohtsu, H.; Itoh, S.; Nagatomo, S.; Kitagawa, T.; Ogo, S.; Watanabe, Y.; Fukuzumi, S. *Inorg. Chem.* **2001**, *40*, 3200–3207. (d) Fujii, T.; Naito, A.; Yamaguchi, S.; Wada, A.; Funahashi, Y.; Jitsukawa, K.; Nagatomo, S.; Kitagawa, T.; Masuda, H. *Chem. Commun.* **2003**, 2700–2701. (e) Yamaguchi, S.; Nagatomo, S.; Kitagawa, T.; Funahashi, Y.; Ozawa, T.; Jitsukawa, K.; Masuda, H. *Inorg. Chem.* **2003**, *42*, 6968–6970. (f) Osako, T.; Nagatomo, S.; Kitagawa, T.; Cramer, C. J.; Itoh, S. *J. Biol. Inorg. Chem.* **2005**, *10*, 581–590. (g) Yamaguchi, S.; Kumagai, A.; Nagatomo, S.; Kitagawa, T.; Funahashi, Y.; Ozawa, T.; Jitsukawa, K.; Masuda, H. *Bull. Chem. Soc. Jpn.* **2005**, *78*, 116–124.

(3) (a) Capdevielle, P.; Maumy, M. *Tetrahedron Lett.* **1990**, *31*, 3891–3892. (b) Chen, P.; Fujisawa, K.; Solomon, E. I. *J. Am. Chem. Soc.* **2000**, *122*, 10177–10193. (c) Ohta, T.; Tachiyama, T.; Yoshizawa, K.; Yamabe, T.; Uchida, T.; Kitagawa, T. *Inorg. Chem.* **2000**, *39*, 4358–4369. (d) Cheruzel, L. E.; Cecil, M. R.; Edison, S. E.; Mashuta, M. S.; Baldwin, M. J.; Buchanan, R. M. *Inorg. Chem.* **2006**, *45*, 3191–3202.

(4) (a) Karlin, K. D.; Ghosh, P.; Cruse, R. W.; Farooq, A.; Gultneh, Y.; Jacobson, R. R.; Blackburn, N. J.; Strange, R. W.; Zubieta, J. *J. Am. Chem. Soc.* **1988**, *110*, 6769–6780. (b) Kodera, M.; Tachi, Y.; Hirota, S.; Katayama, K.; Shimakoshi, H.; Kano, K.; Fujisawa, K.; Morooka, Y.; Naruta, Y.; Kitagawa, T. *Chem. Lett.* **1998**, 389–390. (c) Battaini, G.; Monzani, E.; Perotti, A.; Para, C.; Casella, L.; Santagostini, L.; Gullotti, M.; Dillinger, R.; Näther, C.; Tuczek, F. *J. Am. Chem. Soc.* **2003**, *125*, 4185–4198. (d) Itoh, K.; Hayashi, H.; Furutachi, H.; Matsumoto, T.; Nagatomo, S.; Tosha, T.; Terada, S.; Fujinami, S.; Suzuki, M.; Kitagawa, T. *J. Am. Chem. Soc.* **2005**, *127*, 5212–5223.

(5) (a) Osako, T.; Nagatomo, S.; Tachi, Y.; Kitagawa, T.; Itoh, S. *Angew. Chem., Int. Ed.* **2002**, *41*, 4325–4328. (b) Shimokawa, C.; Teraoka, J.; Tachi, Y.; Itoh, S. *J. Inorg. Biochem.* **2006**, *100*, 1118–1127.

(6) Itoh, S. *Curr. Opin. Chem. Biol.* **2006**, *10*, 115–122.

(7) Itoh, S. In *Comprehensive Coordination Chemistry II*; Que, L., Jr., Tolman, W. B., Eds.; Elsevier: Amsterdam, 2004; Vol. *8*, pp 369−393.

(8) (a) Mirica, L. M.; Ottenwaelder, X.; Stack, T. D. P. *Chem. Rev.* **2004**, *104*, 1013–1045. (b) Lewis, E. A.; Tolman, W. B. *Chem. Rev.* **2004**, *104*, 1047–1076.

(9) Masuda and coworkers have also demonstrated that the substituents at the 6-position of the pyridine nucleus of TPA largely affect the stability and reactivity of the copper(II)-hydroperoxo complexes **A**[1b].

(10) Kunishita, A.; Teraoka, J.; Scanlon, J. D.; Matsumoto, T.; Suzuki, M.; Cramer, C. J.; Itoh, S. *J. Am. Chem. Soc.* **2007**, *129*, 7248–7249.

Chart 2

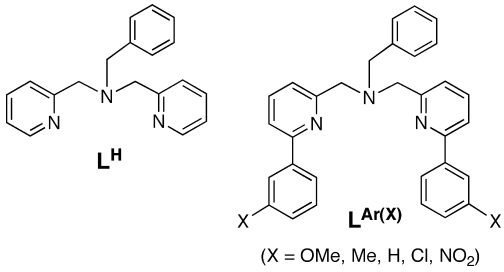

Scheme 1

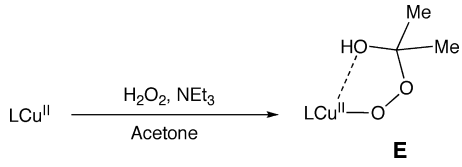

hydroxylation reaction via an electrophilic aromatic substitution mechanism.[10] All these results suggest that more detailed studies of ligand effects, as well as solvent effects, on the reactivity of copper complexes toward H_2O_2 are necessary.

In this work, we have examined in more detail the reaction of copper(II) complexes and H_2O_2 by using the bis(2-pyridylmethyl)amine tridentate ligands L^H and $L^{Ar(X)}$ shown in Chart 2 in both acetone and propionitrile. The results demonstrate that the structure and reactivity of the active-oxygen species generated are significantly affected by both the supporting ligand and the solvent. Theoretical studies at the density functional theory (DFT) level have been employed to provide important insights into the structures and reactivity of the active oxygen species.

Experimental Section

Syntheses. The reagents and the solvents used in this study, except the ligands and the copper complexes, were commercial products of the highest available purity and were further purified by standard methods, as necessary.[11] The copper(II) complexes of ligand $L^{Ar(X)}$, $\mathbf{1^{Ar(X)}}$, were obtained as reported previously.[10] Ligand L^H was synthesized according the reported procedures.[12]

Caution! *The perchlorate salts in this study are all potentially explosive and should be handled with care.*

$[Cu^{II}(L^H)(CH_3CN)_2](ClO_4)_2$ ($\mathbf{1^H}$). $Cu^{II}(ClO_4)_2 \cdot 6H_2O$ (148 mg, 0.40 mmol) was added to an acetonitrile solution (20 mL) of ligand L^H (116 mg, 0.40 mmol). After stirring for 5 min at room temperature, insoluble material was removed by filtration. Addition of ether (100 mL) to the filtrate gave a purple powder that was precipitated by standing the mixture for several minutes. The supernatant was then removed by decantation, and the remained purple solid was washed with ether three times and dried to give complex $\mathbf{1^H}$ in 88%. Micro crystals of $\mathbf{1^H}$ were obtained by vapor diffusion of ether into an acetonitrile solution of the complex. FT-IR (KBr) 1094 and 625 cm^{-1} (ClO_4^-); HRMS (FAB^+) m/z = 451.0348, calcd for $C_{19}H_{19}ClCuN_3O_4$ = 451.0360; Anal. Calcd for $[Cu^{II}(L_3^H)(CH_3CN)_2](ClO_4)_2(C_{23}H_{25}Cl_2CuN_5O_8)$: C, 43.58; H, 3.97; N, 11.05. Found: C, 43.74; H, 3.93; N, 11.12.

$[Cu^{II}(L^H)(OAc)](ClO_4)$ ($\mathbf{6^H}$). An acetone solution (100 mL) of $\mathbf{1^H}$ (126.6 mg, 2.0 mM) was cooled down to −80 °C using a dry ice−AcOEt bath. Then, 30% H_2O_2 aqueous solution (10 equiv) and Et_3N (2 equiv) were added to the solution. The resulting mixture was stirred for 2 h at −80 °C and then gradually warmed up to room temperature. After stirring for additional 30 min at room temperature, the solvent was reduced under reduced pressure to give a blue residue, to which ether (100 mL) was added. Standing the mixture for several minutes in a glovebox resulted in the precipitation of a blue powder. The supernatant was then removed by decantation, and the remaining green-brown solid was washed with ether three times and dried to give $\mathbf{6^H}$ in an 85% yield. FT-IR (KBr) 1605, 1561 (OAc^-), 1088, and 625 cm^{-1} (ClO_4^-); HRMS (FAB, pos) m/z = 411.1008 (M^+); calcd for $C_{21}H_{22}CuN_3O_2$ 411.1008; ESI-MS m/z = 411.12 ($C_{21}H_{22}CuN_3O_2$); Anal. Calcd for $[Cu^{II}(L^H)(OAc)](ClO_4)$ ($\mathbf{6^H}$) ($C_{21}H_{29}ClCuN_3O_{9.5}$): C, 43.91; H, 5.09; N, 7.31. Found: C, 43.71; H, 4.89; N, 7.77. Isotope labeling experiments were performed using $H_2{}^{18}O_2$ instead of $H_2{}^{16}O_2$ [ESI-MS m/z = 413.09 ($C_{21}H_{22}CuN_3{}^{16}O^{18}O$)] and using acetone-$d_6$ instead of acetone-h_6 [ESI-MS m/z = 414.19 ($C_{21}H_{19}D_3CuN_3O_2$)] by the same method as described above.

Physical Methods. FT-IR spectra were recorded on a Jasco FTIR-4100, and UV−visible spectra were taken on a Jasco V-570 or a Hewlett-Packard 8453 photo diode array spectrophotometer. ^1H NMR spectra were recorded on a JEOL FT-NMR Lambda 300WB or a JEOL FT-NMR GX-400 spectrometer. Electron spin resonance (ESR) spectra were recorded on BRUKER E-500 spectrometer at −150 °C and were simulated by using Bruker SimFonia (ver. 1.25) on a HP personal computer (Windows XP). Mass spectra were recorded on a JEOL JMS-700T Tandem MS-station mass spectrometer. ESI-MS (electrospray ionization mass spectra) measurements were performed on a PE SCIEX API 150EX or a Micromass LCT spectrometer. Elemental analyses were recorded with a Perkin-Elmer or a Fisons instruments EA1108 Elemental Analyzer.

Resonance Raman scattering was excited at 406.7 nm from Kr^+ laser (Spectra Physics, BeamLok 2060). Resonance Raman scattering was dispersed by a single polychromator (Ritsu Oyo Kogaku, MC-100) and was detected by a liquid nitrogen cooled CCD detector (Roper Scientific, LNCCD-1100-PB). The resonance Raman measurements were carried out using a rotated cylindrical cell thermostatted from −70 to −90 °C by flashing cold liquid nitrogen gas.

Cyclic voltammetric measurements were performed on an ALS-630A electrochemical analyzer in deaerated CH_3CN containing 0.10 M NBu_4ClO_4 as a supporting electrolyte. A Pt working electrode (BAS) was polished with BAS polishing alumina suspension and rinsed with acetone before use. The counter electrode was a platinum wire. The measured potentials were recorded with respect to a $Ag/AgNO_3$ (0.01 M) reference electrode. All electrochemical measurements were carried out in a glovebox filled with Ar gas at 25 °C.

Crystallographic Studies. The single crystal was mounted on a glass-fiber. X-ray diffraction data were collected by a Rigaku RAXIS-RAPID imaging plate two-dimensional area detector using graphite-monochromated Mo Kα radiation (λ = 0.71069 Å) to $2\theta_{max}$ of 55°. All the crystallographic calculations were performed by using the Crystal Structure software package of the Molecular Structure Corporation [Crystal Structure: Crystal Structure Analysis Package version 3.8.1, Molecular Structure Corp. and Rigaku Corp. (2005)]. The structures were solved with SIR92 and refined with CRYSTALS. All non-hydrogen atoms and hydrogen atoms were

(11) Armarego, W. L. F.; Perrin, D. D. In *Purification of Laborator Chemicals*, 4th ed.; Butterworth-Heinemann: Oxford, 1996; pp 176 and 215.
(12) Kawahara, S.; Uchimaru, T. *Chem.—Eur. J.,* **2001**, 2437–2442.

refined anisotropically and isotropically, respectively. Atomic coordinates, thermal parameters, and intramolecular bond distances and angles are deposited in the Supporting Information (CIF file format).

Kinetic Measurements. Kinetic measurements for the oxygenation reaction of copper(II) complexes $\mathbf{1^{Ar(X)}}$ (X = NO_2, Cl, H, Me, OMe) and $\mathbf{1^H}$ were performed using a Hewlett-Packard 8453 photo diode array spectrophotometer with a Unisoku thermostatted cell holder designed for low temperature measurements (USP-203, a desired temperature can be fixed within ±0.5 °C) in acetone and propionitrile at −70 °C and a multiscan double mixing stopped-flow spectrophotometer designed for low-temperature measurements (RSP-1000, Unisoku Co., Ltd.) in acetone at 0 °C. The pseudo-first-order rate constants for the formation and decomposition processes of the intermediate were determined from the plots of ln ΔA versus time based on the time course of the absorption change at λ_{max} due to the intermediate and/or the product.

Computational Methods. All molecular structures were fully optimized using the generalized gradient approximation (GGA) density functional (*m*PWPW91) that combines the exchange functional of Perdew,[13] as modified by Adamo and Barone,[14] with the correlation functional of Perdew and Wang.[15] For efficiency, the benzyl group substituting the tertiary nitrogen of the experimental ligands was truncated to a methyl group in the computational models. In geometry optimizations, atomic orbital basis functions were taken for Cu from the Stuttgart effective core potential and basis set,[16] for N and O from the 6−311G(d) basis,[17] and for C and H from the 6−31G(d) basis.[17] Analytic vibrational frequencies were computed for all stationary points to confirm their natures as minima or transition-state (TS) structures and also to compute thermal contributions to enthalpy and free energy using the ideal-gas, rigid-rotator, harmonic-oscillator approximations.[18] Single-point calculations on gas-phase structures using the implicit polarized continuum solvation model (PCM)[19] were performed to quantify the influence of solvation on the free energy. Single-point gas-phase calculations were also performed using the M06L functional[20] to examine the sensitivity to the density functional in certain instances.

Results and Discussion

Characterization of Copper(II) Starting Materials. The copper(II) starting materials $\mathbf{1^H}$ and $\mathbf{1^{Ar(X)}}$ supported by L^H and $L^{Ar(X)}$ (see Chart 2), respectively, were efficiently prepared by mixing the ligand and $Cu^{II}(ClO_4)_2 \cdot 6H_2O$ in acetonitrile. The crystal structure of $\mathbf{1^H}$ is shown in Figure 1 together with the crystallographic data and the selected bond lengths and angles presented in Tables 1 and 2, respectively. Crystal structures of $\mathbf{1^{Ar(X)}}$ (X = Me, H, Cl, and NO_2) have already been communicated.[10]

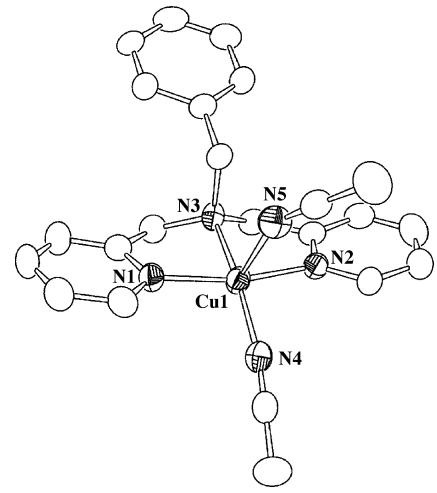

Figure 1. ORTEP drawing of $\mathbf{1^H}$ showing 50% probability thermal ellipsoids. The counteranion and the hydrogen atoms are omitted for clarity.

Table 1. Summary of the X-ray Crystallographic Data of Compound $\mathbf{1^H}$

compound	$\mathbf{1^H}$
formula	$C_{23}H_{25}N_5CuCl_2O_8$
formula weight	633.93
crystal system	monoclinic
space group	*C*2/*c*(#15)
a, Å	25.19(3)
b, Å	10.717(11)
c, Å	21.45(2)
α, deg	90
β, deg	99.5(5)
γ, deg	90
V, Å^3	5709.5(113)
Z	8
F(000)	2600.00
D_{calcd}, g/cm^{-3}	1.475
T, K	153
crystal size, mm	0.20 × 0.20 × 0.20
μ(Mo Kα), cm^{-1}	10.049
$2\theta_{max}$, deg	54.9
no. of reflns measd.	26036
no. of reflns obsd.	4021([$I > 1.00\sigma(I)$])
no. of variables	374
R [a]	0.0550
R_w [b]	0.0778
GOF	1.000

[a] $R = \sum||F_o| - |F_c||/\sum|F_o|$. [b] $R_w = [\sum w(|F_o| - |F_c|)^2/\sum wF_o^2]^{1/2}$.

Table 2. Selected Bond Lengths (Å) and Angles (deg) of Compound $\mathbf{1^H}$

Compound $\mathbf{1^H}$			
Cu(1)−N(1)	1.980(4)	Cu(1)−N(2)	1.978(4)
Cu(1)−N(3)	2.035(4)	Cu(1)−N(4)	1.974(4)
Cu(1)−N(5)	2.439(5)		
N(1)−Cu(1)−N(2)	165.25(18)	N(1)−Cu(1)−N(3)	82.76(16)
N(1)−Cu(1)−N(4)	97.64(18)	N(2)−Cu(1)−N(3)	82.50(17)
N(2)−Cu(1)−N(4)	96.91(18)	N(3)−Cu(1)−N(4)	169.26(18)
N(5)−Cu(1)−N(1)	87.82(17)	N(5)−Cu(1)−N(2)	95.12(17)
N(5)−Cu(1)−N(3)	102.91(15)	N(5)−Cu(1)−N(4)	87.82(17)

Copper(II) complex $[Cu^{II}(L^H)(CH_3CN)_2](ClO_4)_2$ $(\mathbf{1^H})$ exhibits a square pyramidal geometry ($\tau = 0.07$)[21] with the nitrogen atoms, N(1), N(2), and N(3) of L^H and N(4) of one of the acetonitrile co-ligands, occupying the basal plane, and another acetonitrile nitrogen N(5) at the axial position.

(13) Perdew, J. P. In *Electronic Structure of Solids '91*; Ziesche, P., Eschrig, H., Eds.; Akademie Verlag: Berlin, 1991, pp 11−20.
(14) Adamo, C.; Barone, V. *J. Chem. Phys.* **1998**, *108*, 664–675.
(15) Perdew, J.; Wang, Y. *Phys. Rev. B* **1992**, *45*, 13244–13249.
(16) Dolg, M.; Wedig, U.; Stoll, H.; Preuss, H. *J. Chem. Phys.* **1987**, *86*, 866–872.
(17) Hehre, W. J.; Radom, L.; Schleyer, P. v. R.; Pople, J. A. *Ab Initio Molecular Orbital Theory*; Wiley: New York, 1986.
(18) Cramer, C. J. *Essentials of Computational Chemistry: Theories and Models*, 2nd ed.; John Wiley & Sons: Chichester, 2004.
(19) (a) Tomasi, J.; Mennucci, B.; Cances, E. *J. Mol. Struct. (Theochem)* **1999**, *464*, 1211–226. (b) Tomasi, J.; Mennucci, B.; Cammi, R. *Chem. Rev.* **2005**, *105*, 2999–3093.
(20) Zhao, Y.; Truhlar, D. G. *J. Chem. Phys.* **2006**, *125*, 194101.
(21) Addison, A. W.; Rao, T. N.; Reedijk, J.; van Rijn, J.; Verschoor, G. C. *J. Chem. Soc., Dalton Trans.* **1984**, 1349–1356.

Table 3. Redox Potential, UV-vis Data (d-d Band), and ESR Parameters of $\mathbf{1^{H}}$ and $\mathbf{1^{Ar(X)}}$

complex	$E_{1/2}$ (V)[a]	ΔE_p (V)[b]	λ_{max} (ε, M^{-1} cm^{-1})	ESR parameters[c]	
$\mathbf{1^{H}}$	−0.14	0.10	645 nm (150)	$g_1 = 2.260$	$A_1 = 170$ G
				$g_2 = 2.065$	$A_2 = 25$ G
				$g_3 = 2.047$	$A_3 = 18$ G
$\mathbf{1^{Ar(OMe)}}$	0.18	0.10	715 nm (150)	$g_1 = 2.315$	$A_1 = 139$ G
			845 nm (120)	$g_2 = 2.100$	$A_2 = 20$ G
				$g_3 = 2.040$	$A_3 = 24$ G
$\mathbf{1^{Ar(Me)}}$	0.19	0.10	717 nm (170)	$g_1 = 2.315$	$A_1 = 139$ G
			860 nm (150)	$g_2 = 2.103$	$A_2 = 20$ G
				$g_3 = 2.045$	$A_3 = 24$ G
$\mathbf{1^{Ar(H)}}$	0.20	0.10	717 nm (135)	$g_1 = 2.313$	$A_1 = 138$ G
			855 nm (90)	$g_2 = 2.100$	$A_2 = 19$ G
				$g_3 = 2.050$	$A_3 = 25$ G
$\mathbf{1^{Ar(Cl)}}$	0.24	0.12	720 nm (150)	$g_1 = 2.315$	$A_1 = 138$ G
			865 nm (130)	$g_2 = 2.100$	$A_2 = 23$ G
				$g_3 = 2.040$	$A_3 = 24$ G
$\mathbf{1^{Ar(NO2)}}$	0.30	0.10	710 nm (100)	$g_1 = 2.310$	$A_1 = 140$ G
			860 nm (100)	$g_2 = 2.100$	$A_2 = 22$ G
				$g_3 = 2.030$	$A_3 = 24$ G

[a] In CH_3CN containing 0.1 M tetrabutylammonium perchlorate (TBAP) at 25 °C; working electrode Pt, counter electrode Pt, reference electrode Ag/0.01 M $AgNO_3$, sweep rate 50 mV s^{-1}. [b] Peak separation. [c] In CH_3CN at 123 K, microwave frequency 9.40−9.41 GHz, modulation frequency 100 kHz, modulation amplitude 5 G, microwave power 0.20−0.33 mW.

$[Cu^{II}(L^{Ar(H)})(CH_3CN)(ClO_4)](ClO_4)$ ($\mathbf{1^{Ar(H)}}$) showed a similar square pyramidal structure ($\tau = 0.08$) with an acetonitrile molecule occupying the equatorial position and ClO_4^- as the axial co-ligand.[10] It should be noted that the distances between Cu(1) and the pyridine nitrogen atoms N(1) and N(2) in $\mathbf{1^{H}}$, 1.980 and 1.978 Å (see Table 2), are much shorter than those in $\mathbf{1^{Ar(H)}}$, 2,031 and 2.010 Å, whereas the Cu(1)−N(3) and Cu(1)−N(4) distances of $\mathbf{1^{H}}$, 2.035 and 1.974 Å, are longer than those of $\mathbf{1^{Ar(H)}}$, 2,006 and 1.950 Å.[10] Similar structural features [elongation of $Cu(1)-N(1)_{py}$ and $Cu(1)-N(2)_{py}$ distances and shortening of $Cu(1)-N(3)_{amine}$ and $Cu(1)-N(4)_{solv}$ distances] are observed in $\mathbf{1^{Ar(Me)}}$, $\mathbf{1^{Ar(Cl)}}$, and $\mathbf{1^{Ar(NO2)}}$, although their structural distortion from square pyramidal geometry becomes larger ($\tau = 0.45-0.56$).[10] The elongation of the $Cu(1)-N_{py}$ distances in $\mathbf{1^{Ar(X)}}$ as compared with those in $\mathbf{1^{H}}$ can be attributed to the steric repulsion between the cupric ion and the aromatic substituents at the 6-position of pyridine donor groups and/or the repulsion between the aromatic substituents and the co-ligands of $\mathbf{1^{Ar(X)}}$.[22] Such the steric effects of the aromatic substituents makes the electron-donor ability of pyridine in $\mathbf{1^{Ar(X)}}$ weaker than that in $\mathbf{1^{H}}$, which is reflected in the redox potentials described below.

The ESR data of the copper(II) starting materials are summarized in Table 3. The spectra themselves are presented in Supporting Information, Figures S1−S6. The A_1 value (170 G) of complex $\mathbf{1^{H}}$ is a normal one for copper(II) complexes with square pyramidal geometry.[23] Thus, the square pyramidal geometry ($\tau = 0.07$) of $\mathbf{1^{H}}$ in the crystal may be maintained in the solution (frozen CH_3CN). On the other hand, all $\mathbf{1^{Ar(X)}}$ complexes exhibit relatively smaller A_1 values (135−139 G), suggesting that they have a significantly distorted square pyramidal geometry in the solution.[23] Thus, it can be said that the structures of $\mathbf{1^{Ar(Me)}}$, $\mathbf{1^{Ar(Cl)}}$, and $\mathbf{1^{Ar(NO2)}}$ in the solution are similar to those in the crystals ($\tau = 0.45-0.56$), whereas the square pyramidal structure of $\mathbf{1^{Ar(H)}}$ found in the crystal ($\tau = 0.08$) may be significantly distorted toward trigonal bipyramidal in the solution.

The UV−vis spectra of the copper(II) complexes presented in Table 3 support the notion of their solution structures. Namely, complex $\mathbf{1^{H}}$ exhibits a d-d band at 645 nm, which is a typical one for copper(II) complexes with square pyramidal geometry, whereas $\mathbf{1^{Ar(X)}}$ complexes show two d-d bands at ∼710 nm and ∼860 nm, which are characteristics for the distortion of copper(II) toward trigonal bipyramidal geometry.[23]

All copper(II) complexes gave a reversible redox couple ($\Delta E_p \sim 100$ mV) in CH_3CN (Table 3). The cyclic voltammograms are presented in Supporting Information, Figures S7−S12. Apparently, the redox potential of $\mathbf{1^{Ar(X)}}$ is more than 300 mV higher than that of $\mathbf{1^{H}}$. This can be attributed to the weaker electron-donor ability of $L^{Ar(X)}$ as discussed above. With respect to the order of $E_{1/2}$ in the series of $\mathbf{1^{Ar(X)}}$, the electron-withdrawing *m*-substituents such as NO_2 and Cl further weaken the electron-donor ability of pyridine as compared with the electron-donating *m*-substituents such as Me and OMe.

Reaction of Copper(II) Complexes and H_2O_2 in Acetone ($CH_3C(O)CH_3$). As has already been reported,[10] $\mathbf{1^{Ar(X)}}$ readily reacts with H_2O_2 in a 1:1 ratio in acetone at −70 °C in the presence of triethylamine (1 equiv) to produce 2-hydroxy-2-hydroperoxypropane (HHPP) adducts $\mathbf{2^{Ar(X)}}$ (**E** in Scheme 1), which exhibit a relatively intense LMCT band at ∼420 nm ($\varepsilon = \sim 1000$ M^{-1} cm^{-1}) together with a weak d-d band at ∼650 nm ($\varepsilon = \sim 200$ M^{-1} cm^{-1}) (eq 1).[10]

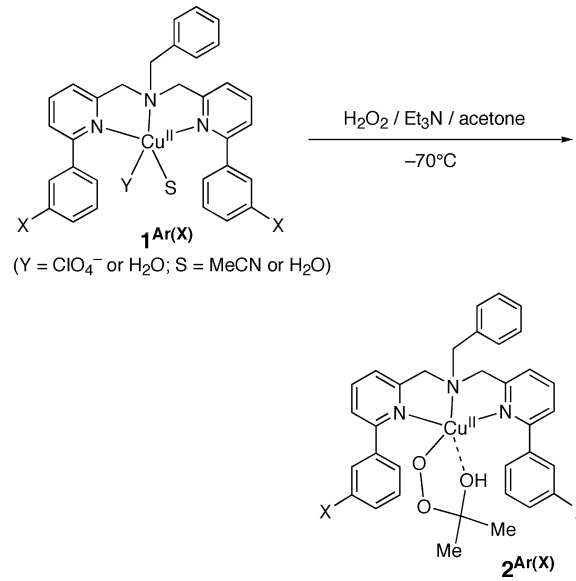

(1)

Intermediate $\mathbf{2^{Ar(NO2)}}$ (X = NO_2), for example, gave isotope sensitive resonance Raman bands at 855, 823, 792, and 545 cm^{-1} in perdeuterated acetone (acetone-d_6), which shifted to 825, 803, 785, and 525 cm^{-1} when $H_2{}^{18}O_2$ was employed instead of $H_2{}^{16}O_2$.[10] Appearance of the multiple Raman bands in the 800 cm^{-1} region and their associated isotope shifts ($\Delta\nu = 30$, 20, and 7 cm^{-1}), as well as their peak intensity

(22) Nagao, H.; Komeda, N.; Mukaida, M.; Suzuki, M.; Tanaka, K. *Inorg. Chem.* **1996**, *35*, 6809–6815.

(23) Mukherjee, R. In *Comprehensive Coordination Chemistry II*; McCleverty, J. A., Meyer, T. J., Eds.; Elsevier: Amsterdam, 2004; Vol. 6, pp 747−910, and references cited therein.

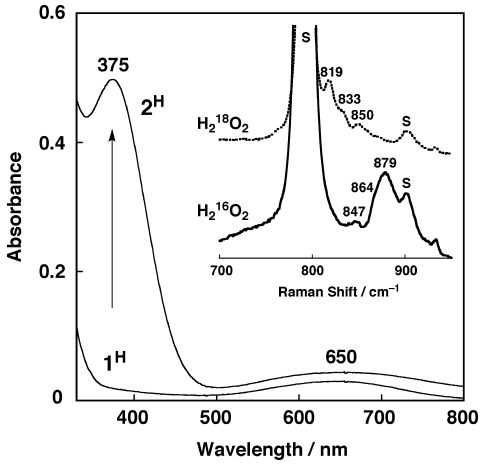

Figure 2. Spectral change for the reaction of $\mathbf{1^H}$ (0.2 mM) with H_2O_2 (2.0 mM) in the presence of NEt_3 (2.0 mM) in acetone at −70 °C. Inset: Resonance Raman spectra of $\mathbf{2^H}$ (5 mM) generated by using $H_2{}^{16}O_2$ (solid line) and $H_2{}^{18}O_2$ (dashed line) obtained with $\lambda_{ex} = 406.7$ nm in acetone at −80 °C; s denotes the solvent bands.

patterns, are very close to the resonance Raman data of the copper(II)-alkylperoxo complexes $LCu^{II}-OOR$ [L = hydrotrispyrazolylborate and R = *tert*-butyl (Bu^t) or cumyl (Cm)] reported by Solomon and co-workers and also to those of the iron(III)-alkylperoxo complex $LFe^{III}-OOBu^t$ (L = TPA derivatives) reported by Que and co-workers.[3b,24] By analogy to those resonance Raman data of the related alkylperoxo complexes,[3b,24] the multiple Raman bands around 800 cm^{-1} of $\mathbf{2^{Ar(NO2)}}$ can be assigned as mixed O−O/C−O/C−C vibrations. Then, the Raman band at 545 cm^{-1} can be attributed to the Cu−O stretching vibration. ESR and ESI-MS studies unambiguously support the formation of $\mathbf{2^{Ar(NO2)}}$.[10] A similar HHPP-adduct of iron(III) has been reported by Que and co-workers in the reaction of Fe^{II}(TPA) and H_2O_2 in acetone.[25,26]

The reaction of $\mathbf{1^H}$ without the 6-phenyl substituent and H_2O_2 has also been examined under the same experimental conditions. The spectral change for the reaction is shown in Figure 2, where a relatively intense absorption band at 375 nm ($\varepsilon = 2500$ M^{-1} cm^{-1}) appears together with a weak d-d band at 650 nm (220 M^{-1} cm^{-1}). The spectrum is quite different from that of Masuda's copper(II)-hydroperoxo complex $LCu^{II}-OOH$ (**A**) generated by using a similar bis(2-pyridylmethyl)amine ligand $L^{H(Bu)}$ having a *tert*-butyl *N*-substituent (see Chart 3) in acetone; $\lambda_{max} = 350$ nm (ε = 3400 M^{-1} cm^{-1}), 564 (150), and 790 (55).[2d]

The resonance Raman features of our intermediate are also different from those of Masuda's $LCu^{II}-OOH$ complex of $L^{H(Bu)}$. Namely, our intermediate showed multiple Raman bands at 879, 864, and 847 cm^{-1}, which shifted to 850, 833, and 819 cm^{-1} upon ^{18}O-substitution as shown in the inset

Chart 3

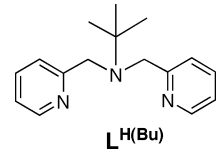

$L^{H(Bu)}$

of Figure 2, whereas Masuda's hydroperoxo copper(II) complex exhibits only a single Raman band at 834 cm^{-1} assigned to the $^{16}O-^{16}O$ stretching vibration.[2d] These results strongly suggest the generation of an HHPP-adduct $\mathbf{2^H}$ (**E**) in analogy to the $\mathbf{2^{Ar(X)}}$ examples (eq 2). Incorporation of an acetone molecule into $\mathbf{2^H}$ was confirmed by noting that the multiple Raman bands at 850, 833, and 820 cm^{-1} of $\mathbf{2^H}$, generated by the reaction with $H_2{}^{18}O_2$ in acetone-h_6, were shifted to 829, 814, and 793 cm^{-1} when the sample was generated in acetone-d_6 (Supporting Information, Figure S13).[27] The reason for the difference in reactivity between our system and that of the Masuda's system is not obvious at present.

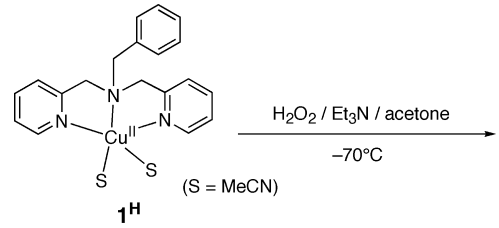

$\mathbf{1^H}$ (2)

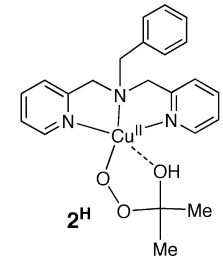

$\mathbf{2^H}$

The ESR spectrum of $\mathbf{2^H}$ shown in Figure 3, which is different from that of the starting material $\mathbf{1^H}$ (see Table 3), indicates that intermediate $\mathbf{2^H}$ also has a tetragonal geometry.[23] Moreover, double integration of the ESR spectrum of $\mathbf{2^H}$ indicated that 98% of the spin remained, confirming the mononuclearity of $\mathbf{2^H}$ as in the case of $\mathbf{2^{Ar(X)}}$.[10]

Reactivity of HHPP-Adducts 2. The HHPP-adducts $\mathbf{2^{Ar(X)}}$ have previously been shown to undergo an aromatic ligand hydroxylation reaction, giving phenolate-copper(II) product complexes $\mathbf{4^{Ar(X)}}$ (eq 3).[10] Isotope labeling experiments using $H_2{}^{18}O_2$ unambiguously indicated that the origin of the phenolate oxygen in the products was hydrogen peroxide, and X-ray analysis on a single crystal of $\mathbf{4^{Ar(X)}}$ confirmed the position of the hydroxylation reaction (*para* to the substituent X, see eq 3).[10] Demetalation of $\mathbf{4^{Ar(X)}}$ by an

(24) (a) Zang, Y.; Elgren, T. E.; Dong, Y.; Que, L., Jr *J. Am. Chem. Soc.* **1993**, *115*, 811–813. (b) Zang, Y.; Kim, J.; Dong, Y.; Wilkinson, E. C.; Appelman, E. H.; Que, L., Jr *J. Am. Chem. Soc.* **1997**, *119*, 4197–4205.

(25) Payeras, A. M.; Ho, R. Y. N.; Fujita, M.; Que, L., Jr *Chem.—Eur. J.* **2004**, *10*, 4944>4953.

(26) The reversible addition of H_2O_2 to acetone to form 2-hydroxy-2-hydroperoxypropane (HHPP) was first studied in detail by (a) Sauer, M. C. V.; Edwards, J. O. *J. Phys. Chem.* **1971**, *75*, 3004–3011.

(27) The low temperature ESI-MS measurement gave a set of peaks at $m/z = 443.1$ with $H_2{}^{16}O_2$ that shifts to 447.1 upon $H_2{}^{18}O_2$ substitution (Supporting Information, Figure S14). The mass distribution patterns about these peaks, as well as their isotope shifts, are fully consistent with the HHPP-adduct structure of copper(II) complex $\mathbf{2^H}$. However, the mass data also fit the structures of suggested intermediates $\mathbf{5^H}$ and $\mathbf{5a^H}$ shown in Figure 7.

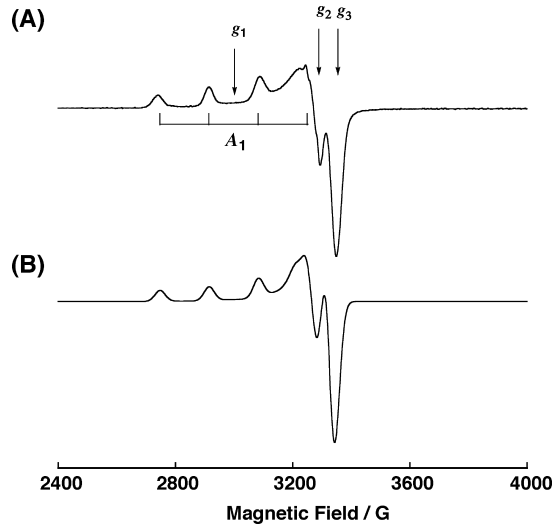

Figure 3. (A) ESR spectrum of $\mathbf{2^H}$ and (B) the computer simulation spectrum with the parameters $g_1 = 2.240$, $g_2 = 2.052$, $g_3 = 2.060$, $A_1 = 168.0$ G, $A_2 = 32.0$ G, and $A_3 = 3.0$ G.

ordinary workup treatment using NH_4OH(aq) gave the hydroxylated ligands $L^{Ar(X)-OH}$ in yields of 99% for X = OMe, 98% for X = Me, 85% for X = H, 99% for X = Cl, and 53% for X = NO_2.[10]

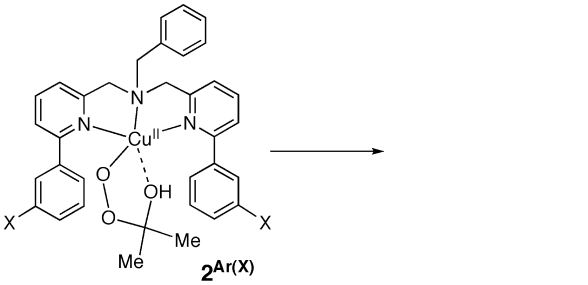

(3)

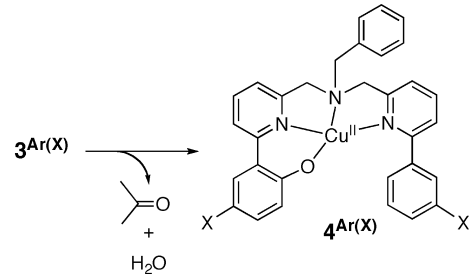

During the course of the reaction from $\mathbf{2^{Ar(X)}}$ to $\mathbf{4^{Ar(X)}}$, another intermediate $\mathbf{3^{Ar(X)}}$ having a rather featureless UV−vis spectrum was detected (eq 3).[10] The conversion of $\mathbf{2^{Ar(X)}}$ to $\mathbf{3^{Ar(X)}}$ obeyed first-order kinetics, and from the temperature dependence of the decay rate we obtained the activation parameters $\Delta H^{\ddagger} = 24.9 \pm 1.2$ kJ mol^{-1} and $\Delta S^{\ddagger} = -162.9 \pm 5.5$ J K^{-1} mol^{-1}.[10] Furthermore, Hammett analysis (plot of log k_{obs} vs σ^+) gave $\rho = -2.2$ ($r^2 = 0.99$), which is very close to other ρ values reported for aromatic hydroxylation reactions of dicopper(II)-peroxo complexes (−1.8 to −2.2).[28−30] In addition, a negative deuterium kinetic isotope effect (KIE) (KIE = 0.9 ± 0.02; $k_H = 5.0 \times 10^{-3}$ s^{-1} and $k_D = 5.5 \times 10^{-3}$ s^{-1}) was obtained using the perdeuterated ligand L^H-d_{10} (replacing all protons of the 6-phenyl groups), suggesting that the rate-limiting step does not involve proton migration from the phenyl substituent of $\mathbf{3^{Ar(X)}}$ but instead involves a conversion of sp^2 aromatic carbon to sp^3 carbon.[31] These kinetic results suggest that the reaction of $\mathbf{2^{Ar(X)}}$ to $\mathbf{3^{Ar(X)}}$ involves an electrophilic attack by the peroxo moiety to the phenyl substituent at the 6-position of pyridine, leading the C−O bond formation.

At the *m*PWPW91 level of theory, we located a TS structure for an electrophilic aromatic substitution whereby $\mathbf{2^{Ar(H)}}$ reacts to form the intermediate complex $\mathbf{3^{Ar(H)}}$ (Figure 4). The TS structure has a forming C−O bond of 1.800 Å and a breaking O−O bond of 1.504 Å. The interaction between the Cu atom and the O atom being transferred remains strong, as evidenced by a Cu−O bond length of 1.935 Å. The other two O atoms of the HHPP fragment are 2.540 and 2.799 Å distant from the Cu atom, suggesting only weak interactions with the metal. The enthalpy of activation (including solvation free energy) is computed to be 98.0 kJ/mol, which is in quite poor agreement with the experimental enthalpy of activation of 24.9 kJ/mol (vide supra). However, the product immediately deriving from the aromatic hydroxylation is predicted to be the intermediate $\mathbf{3^{Ar(H)}}$, which, relative to $\mathbf{2^{Ar(H)}}$, has shifted a proton from the original hydroxyl group of the HHPP moiety to the now acetal oxygen atom derived from breaking the O−O bond. This suggests that the ring hydroxylation reaction should be catalyzed by general acid or base catalysis to either remove the proton from the original hydroxyl group or donate a proton to the distal oxygen of the peroxy fragment (making the acetal a better leaving group in what may be viewed as a nucleophilic attack by the aromatic ring on the other proximal peroxy oxygen atom), or both as illustrated in Scheme 2.

Indeed, when the same reaction coordinate is computed with an ammonium ion (R = H in Scheme 2) as a proton donor to the distal oxygen of the peroxy fragment, the enthalpy of activation is predicted to decrease to 56.6 kJ/mol, and, when an ammonia molecule (R = H in Scheme 2) is added to act as a base and accept the hydroxyl proton, the activation enthalpy is reduced to 9.0 kJ/mol. In the TS structure for this final case, the hydroxyl proton is not in flight to the ammonia acceptor but there is a strong hydrogen bond facilitating the reaction. In the experimental reaction system, the conjugate acid/base pair is likely to be triethylammonium/triethylamine (R = Et in Scheme 2). The greater steric bulk of these species may rationalize the greater experimental enthalpy of activation (24.9 kJ/mol) compared to that obtained by computation, but theory makes clear that protonation of the peroxy species can significantly accelerate the ring hydroxylation, in a fashion analogous to the mechanism proposed for the formation of the active iron-

(28) Itoh, S.; Kumei, H.; Taki, M.; Nagatomo, S.; Kitagawa, T.; Fukuzumi, S. *J. Am. Chem. Soc.* **2001**, *123*, 6708–6709.
(29) Palavicini, S.; Granata, A.; Monzani, E.; Casella, L. *J. Am. Chem. Soc.* **2005**, *127*, 18031–18036.
(30) Matsumoto, T.; Furutachi, H.; Kobino, M.; Tomii, M.; Nagatomo, S.; Tosha, T.; Osako, T.; Fujinami, S.; Itoh, S.; Kitagawa, T.; Suzuki, M. *J. Am. Chem. Soc.* **2006**, *128*, 3874–3875.
(31) In our previous communication,[10] KIE was reported as 1.0. However, multiple re-examinations gave a negative KIE as 0.9 ± 0.02.

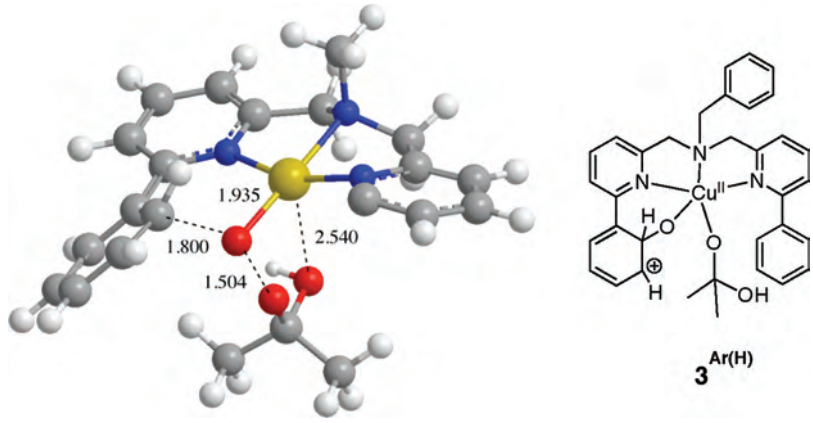

Figure 4. The *m*PWPW91 computed TS structure is shown at left with selected bond lengths (Å); the atoms of the 6-pyridyl phenyl ring that is not reacting have been deleted for clarity. The product derived from the reaction, assigned as $\mathbf{3}^{\mathbf{Ar(H)}}$, is shown at right. In the ball-and-stick structure, the Cu atom is bronze, the O atoms red, the N atoms blue, the C atoms gray, and the H atoms white.

Scheme 2

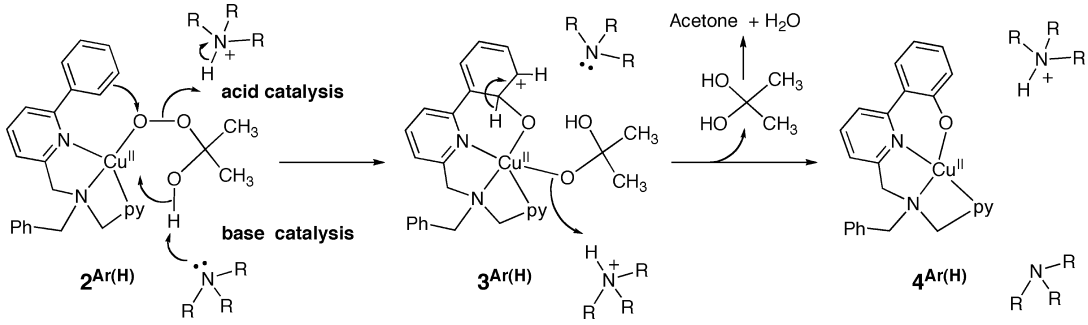

oxo species in horseradish peroxidase, for instance.[32] M06L single point calculations on the relevant structures for the uncatalyzed, protonated, and proton-shuttle facilitated reactions predict enthalpies of activation (including solvation) of 105.7, 59.1, and 8.7 kJ/mol, respectively, suggesting little sensitivity to the functional for the modeling of ring oxidation. Finally, the large, negative entropy of activation observed experimentally ($\Delta S^{\ddagger} = -162.9 \pm 5.5$ J K^{-1} mol^{-1}) is consistent with our proposal of general acid/base catalysis.

When the ammonia/ammonium ion pair is included in the computation of the aromatic hydroxylation, the product deriving from the TS structure is observed to have undergone a spontaneous 1,2-hydride shift from the oxygenated position to the adjacent carbocation (see Scheme 2). Thus, the UV spectrum observed for the $\mathbf{3}^{\mathbf{Ar(X)}}$ species may be for cyclohexadienone intermediates rather than carbocationic intermediates. In either case, however, rearomatization of intermediate $\mathbf{3}^{\mathbf{Ar(H)}}$ can be accomplished by proton transfer to either amine base or the dimethoxyacetal anion (whether intra- or intermolecularly), leading, upon hydrolysis of the acetal, to the final product $\mathbf{4}^{\mathbf{Ar(H)}}$, acetone, and water (Scheme 2). The net driving force for this conversion is very large, with a computed exergonicity of about −344 kJ/mol at 298 K. In support of this mechanism, KIE = 1.5 ($k_H = 3.8 \times 10^{-2}$ s^{-1} and $k_D = 2.6 \times 10^{-2}$ s^{-1}) was experimentally obtained in the transformation process from $\mathbf{3}^{\mathbf{Ar(H)}}$ to $\mathbf{4}^{\mathbf{Ar(H)}}$, when perdeuterated ligand L^H-d_{10} was employed instead of L^H.

The HHPP-adduct $\mathbf{2}^{\mathbf{H}}$ reported here, in contrast to $\mathbf{2}^{\mathbf{Ar(X)}}$, cannot undergo aromatic hydroxylation. Instead it decomposed gradually at −70 °C ($k_{dec} = 8.2 \times 10^{-3}$ s^{-1}) to give the copper(II)-acetate complex $[Cu^{II}(L^H)(OAc)](ClO_4)$ ($\mathbf{6}^{\mathbf{H}}$). Product analysis on a scale-up reaction (2.0 mM) gave $\mathbf{6}^{\mathbf{H}}$ in a 85% yield. Isotope labeling experiments using $H_2{}^{18}O_2$ demonstrated that one of the oxygen atoms of the acetate ion originated from hydrogen peroxide as shown in the inset of Figure 5. Formation of acetate from the HHPP-adduct of Fe^{III}(TPA) has also been reported by Que et al.[25]

In this case, *m*PWPW91 calculations suggest that a plausible mechanism (Figure 6) involves a tautomerization

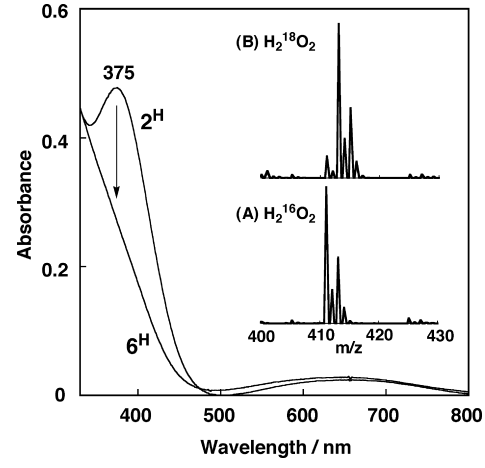

Figure 5. Spectral change for the decomposition of $\mathbf{2}^{\mathbf{H}}$ (0.2 mM) in acetone at −70 °C. Inset: ESI-MS spectra of $\mathbf{6}^{\mathbf{H}}$ generated (A) by using $H_2{}^{16}O_2$ and (B) by using $H_2{}^{18}O_2$.

(32) Newmyer, S. L.; Ortiz de Montellano, P. R. *J. Biol. Chem.* **1995**, *270*, 19430.

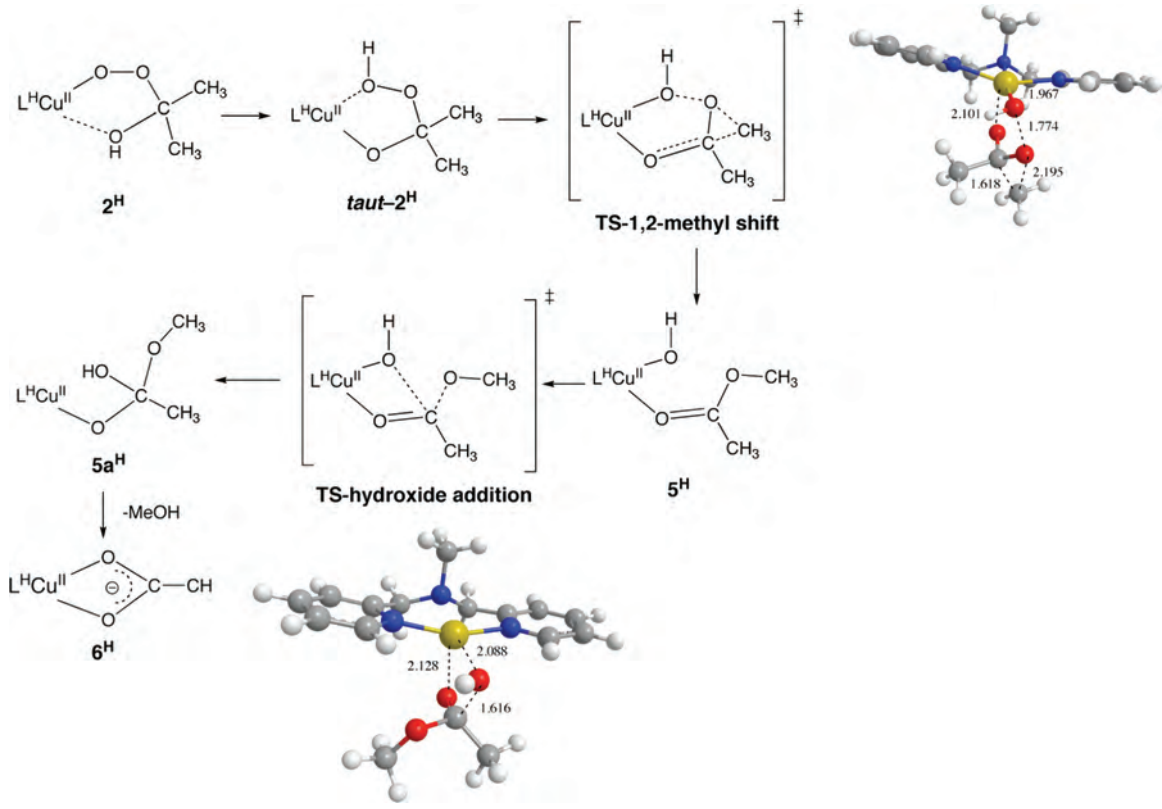

Figure 6. Reaction mechanism for the conversion of $\mathbf{2^H}$ to $\mathbf{6^H}$. Optimized geometries for the two TS structures are shown with selected bond lengths (Å). See Figure 4 for atom color codes.

of the HHPP ligand to protonate the hydroperoxy moiety instead of the hydroxide. This tautomer **taut-2^H** is predicted to be higher in free energy (including solvation) by about 80.5 kJ/mol at 203 K. From this tautomer, a TS structure for a Baeyer−Villiger type 1,2-methyl shift was found in which the breaking of the O−O bond is advanced (1.775 Å) relative to the breaking C−C bond (1.618 Å), and the incipient hydroxide interacts strongly with the copper atom, with a Cu−O bond length of 1.967 Å. The free energy of activation for this process was computed to be 11.3 kJ/mol relative to the tautomerized intermediate, or 91.8 kJ/mol relative to $\mathbf{2^H}$. The interpretation of the experimentally observed decomposition rate constant ($k_{dec} = 8.2 \times 10^{-3}$ s^{-1}) using TS theory for a unimolecular process suggests a free energy of activation of 57.2 kJ/mol at 203 K, which is lower than the value predicted from the *m*PWPW91 calculations. As noted above for ring oxidation, however, this reaction would likely be significantly facilitated by employing an external base/conjugate acid pair to accomplish the proton shuttling rather than enforcing tautomerization as an initial step; we did not, however, search for such structures specifically in this case. In addition, this reaction does show some sensitivity to the functional employed: at the M06L level the 203 K free energy of activation including solvation is predicted to be 77.0 kJ/mol, which is considerably closer to the experimental value (57.2 kJ/mol).

The coordinated hydroxyl group in intermediate $\mathbf{5^H}$, which is −213.2 kJ/mol more stable than the initial reactant $\mathbf{2^H}$ at the *m*PWPW91 level, can subsequently nucleophilically attack the carbonyl carbon of the coordinated methyl acetate to generate a copper-coordinated hemiorthoacetate. Theory predicts the energies of the TS and orthoester product structures to be −143.0 and −181.2 kJ/mol relative to $\mathbf{2^H}$ (the free energy of activation for the ester hydrolysis is thus 70.2 kJ/mol). In the TS structure for nucleophilic addition, the breaking and making Cu−O bond lengths are similar, 2.088 and 2.128 Å, respectively. We did not attempt to determine a precise pathway for breakdown of the orthoester to coordinated acetate and methanol (many different alternatives involving intra- and intermolecular proton transfer are obviously possible and would be expected to occur with very low barrier). We did compute the net exergonicity for the entire reaction of $\mathbf{2^H}$ to $\mathbf{6^H}$, and this is −295.5 kJ/mol at the solvated *m*PWPW91 level.

Another potential pathway for decomposition was considered, namely a 1,3-methyl shift to generate methoxide and acetic acid ligands directly. However, no reasonable TS structures could be found for this process starting from $\mathbf{2^H}$—only very high-energy species with the methyl group migrating essentially as a free methyl radical could be located.[33] Even after deprotonation of the hydroxyl group by triethylamine to make the acetate a better leaving group, free energies of activation of about 200 kJ/mol were computed. Transfer of the proton from the HHPP hydroxyl group to the peroxyl oxygen that is *not* bonded to copper leads to spontaneous C−O bond cleavage to regenerate the original hydroperoxycopper acetone complex. On that basis, we consider the Baeyer−Villiger type 1,2-methyl shift to be more likely than the 1,3-methyl shift to explain the observed reactivity of $\mathbf{2^H}$. However, we cannot rule out the

possibility that a proton shuttle like that implicated in ring hydroxylation might not make the 1,3-methy shift pathway accessible.

Reaction of Copper(II) Complexes and H_2O_2 in Propionitrile (CH_3CH_2CN). The reaction of $\mathbf{1}^{\mathbf{Ar(H)}}$ and H_2O_2 in *propionitrile* under otherwise the same experimental conditions (at −70 °C in the presence of 1 equiv of Et_3N) gave a spectrum exhibiting an intense absorption band at 360 nm (ε = 3150 M^{-1} cm^{-1}, Figure 7), which is quite different from that of $\mathbf{2}^{\mathbf{Ar(H)}}$ (λ_{max} = 420 nm, ε = 1100 M^{-1} cm^{-1}).[10] Although the instability of this intermediate $\mathbf{7}^{\mathbf{Ar(H)}}$ did not permit detailed characterization by ESR, resonance Raman, and ESI-mass spectra (decomposition rate $k_{dec} = 2.4 \times 10^{-2}$ s^{-1} at −70 °C), we assume that $\mathbf{7}^{\mathbf{Ar(H)}}$ is a simple hydrogen peroxide adduct LCu^{II}−OOH (Type **A**) as in the reaction of $\mathbf{1}^{\mathbf{H}}$ and H_2O_2 in propionitrile shown below.

Interestingly, decomposition of $\mathbf{7}^{\mathbf{Ar(H)}}$ resulted in a color change of the solution from green to pale yellow; the d-d bands due to the copper(II) complex in the visible region were completely bleached (see Figure 7), and a copper(I) complex of $L^{Ar(H)}$ ($\mathbf{8}^{\mathbf{Ar(H)}}$) was obtained as the final product (Supporting Information, Figure S15). In this case, the original ligand was recovered nearly quantitatively (no ligand modification). These results clearly indicate that LCu^{II}−OOH species supported by $L^{Ar(H)}$ ($\mathbf{7}^{\mathbf{Ar(H)}}$) have neither arene hydroxylation ability nor aliphatic C−H bond activation ability but instead undergo Cu^{II}−O bond homolysis to give the copper(I) product $\mathbf{8}^{\mathbf{Ar(H)}}$ (eq 4). This result is in sharp contrast to the reactions of Karlin's TPA system, where aromatic hydroxylation as well as oxidative *N*-dealkylation reactions took place in the reactions of copper(II) complexes and H_2O_2 in acetone.[1d,e]

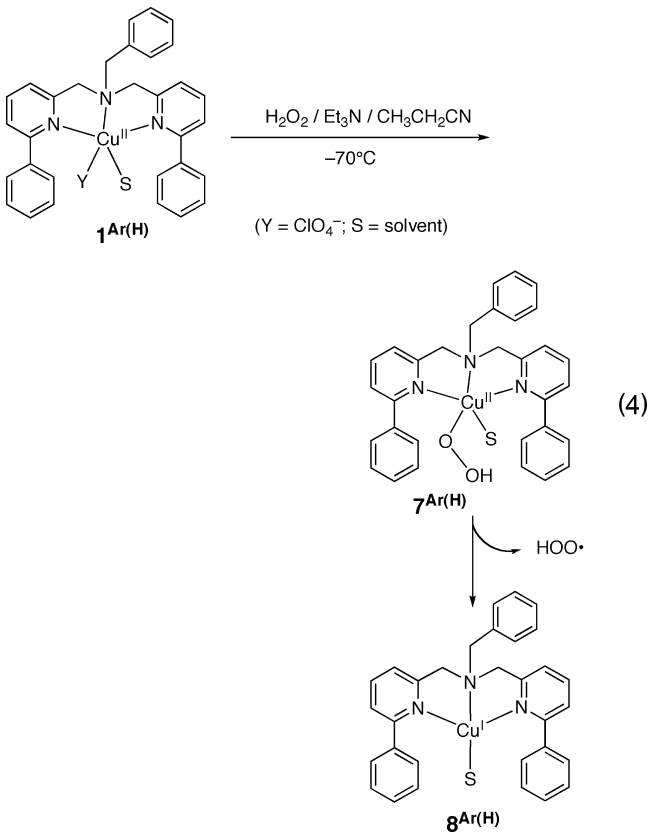

(4)

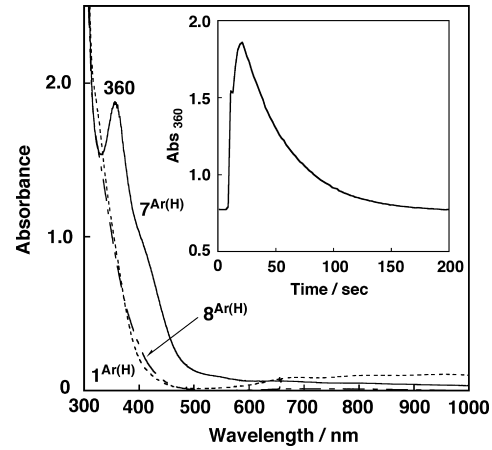

Figure 7. Spectral change for the reaction of $\mathbf{1}^{\mathbf{Ar(H)}}$ (0.6 mM) with H_2O_2 (0.6 mM) in the presence of Et_3N (0.6 mM) in CH_3CH_2CN at −70 °C. Inset: the time course of the absorption change at 360 nm.

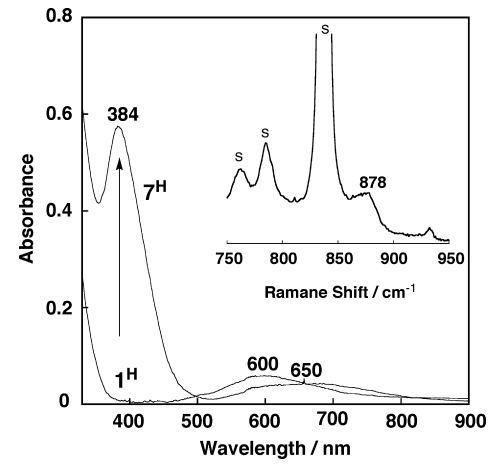

Figure 8. Spectral change for the reaction of $\mathbf{1}^{\mathbf{H}}$ (0.2 mM) with H_2O_2 (2.0 mM) in the presence of Et_3N (2.0 mM) in propionitrile at −70 °C. Inset: Resonance Raman spectrum of $\mathbf{7}^{\mathbf{H}}$ (5 mM) generated by using $H_2{}^{16}O_2$ obtained with λ_{ex} = 406.7 nm in propionitrile at −80 °C, s denotes the solvent peaks.

The reaction of $\mathbf{1}^{\mathbf{H}}$ and H_2O_2 in propionitrile also gave an intense absorption band at 384 nm (ε = 2850 M^{-1} cm^{-1}, Figure 8), which is also different from that of the HHPP-adduct $\mathbf{2}^{\mathbf{H}}$ (Figure 2). In this case, the hydroperoxo copper(II) LCu^{II}−OOH ($\mathbf{7}^{\mathbf{H}}$) could be detected by its resonance Raman spectrum, which exhibited a peak at 878 cm^{-1} attributable to the O−O stretching vibration, although the isotope shift could not be detected because of the overlap of the ^{18}O−^{18}O stretching vibration peak with the large solvent peak around 840 cm^{-1} (see inset of Figure 8).

Conclusions

The reaction of copper(II) complexes $\mathbf{1}^{\mathbf{H}}$ and $\mathbf{1}^{\mathbf{Ar(X)}}$ supported by the bis(2-pyridylmethyl)amine derivatives (L^H and $L^{Ar(X)}$, respectively, see Chart 2) and H_2O_2 have been examined in detail. Both complexes provided 2-hydroxy-2-hydroperoxypropane (HHPP) adduct complexes $\mathbf{2}^{\mathbf{H}}$ and $\mathbf{2}^{\mathbf{Ar(X)}}$ in acetone, whose formation has been confirmed by UV−vis, resonance Raman, ESR, and ESI-MS spectra. In the case of $\mathbf{2}^{\mathbf{Ar(X)}}$, aromatic ligand hydroxylation took place to give the phenolate-copper(II) product complexes $\mathbf{4}^{\mathbf{Ar(X)}}$ in good yields,

during the course of which another intermediate $\mathbf{3}^{\mathbf{Ar(X)}}$ was also detected. Kinetic studies including deuterium KIE and Hammett analysis of the reaction have indicated that the reaction process from $\mathbf{2}^{\mathbf{Ar(X)}}$ to $\mathbf{3}^{\mathbf{Ar(X)}}$ involves C−O bond formation between the peroxo moiety of $\mathbf{2}^{\mathbf{Ar(X)}}$ and one of the phenyl substituents on the pyridine donor groups through an electrophilic aromatic substitution mechanism. Our DFT calculations suggest that this C−O bond formation is significantly facilitated by ammonium/amine acid/base catalysis. Such an acid/base catalysis not only enhances the heterolytic O−O bond cleavage necessary for the electrophilic attack by the peroxo moiety on the aromatic ring of the ligand but also makes the acetal a better leaving group. The relative importance of the ultimate deprotonation from the hydroxyl group of the HHPP moiety in $\mathbf{2}^{\mathbf{Ar(X)}}$ for the aromatic ligand hydroxylation is evident, since no such ligand hydroxylation occurred in a simple alkylperoxo complex LCu^{II}−OOCm (Cm = cumyl) supported by the same tridentate ligand.[34]

In contrast to adducts having the opportunity to oxidize aromatic ring substituents, another HHPP-adduct $\mathbf{2}^{\mathbf{H}}$ gave a copper(II)-acetate complex $\mathbf{6}^{\mathbf{H}}$, in which the acetate co-ligand was derived from the HHPP moiety via a Baeyer−Villiger-like 1,2-methyl shift and subsequent hydrolysis of the methyl acetate so generated by the LCu^{II}−OH species. In this case, DFT calculations again suggested that proton migration in the HHPP moiety from the hydroxyl group to the peroxo group is important and is facilitated by amine/ammonium acid/base catalysis.

In propionitrile as the solvent under otherwise identical reaction conditions with H_2O_2, simple copper(II)-hydroperoxo complexes $\mathbf{7}^{\mathbf{H}}$ and $\mathbf{7}^{\mathbf{Ar(X)}}$ were produced. From these complexes no ligand modification took place, which is an interesting contrast with the TPA systems of Karlin, where otherwise analogous LCu^{II}−OOH species have been reported to undergo both aromatic hydroxylation and oxidative *N*-dealkylation of the supporting ligands.[1d,e]

Our results thus highlight the significant sensitivities to solvent and ligand variation that are exhibited by reactions between the copper(II) complexes and H_2O_2. In addition, our computational work suggests that acid/base catalysis can play a significant role in the O−O bond activation of reactive LCu^{II}−OOR species.

Acknowledgment. This work was financially supported in part by Grants-in-Aid for Scientific Research on Priority Area (Nos. 18033045, 19020058, 19027048, and 19028055 for S.I.) and by Global Center of Excellence (GCOE) Program ("Picobiology: Life Science at Atomic Level" to T.O.) from MEXT, Japan. The U.S. National Science Foundation also provided funding (CHE-0610183).

Supporting Information Available: The ERS spectra (Figures S1−S6) and the cyclic voltammograms (Figures S7−S12) of the copper(II) starting materials, the resonance Raman spectrum of $\mathbf{2}^{\mathbf{H}}$ generated by using $H_2{}^{18}O_2$ in acetone-d_6 (Figure S13), the ESI-MS of $\mathbf{2}^{\mathbf{H}}$ (Figure S14) and $\mathbf{8}^{\mathbf{Ar(H)}}$ (Figure S15), and atomic coordinates for the computed structures (Table S1). This material is available free of charge via the Internet at http://pubs.acs.org.

IC800845H

(33) In the case of the HHPP-adduct of Fe^{III}(TPA), the formation of acetate product was suggested to involve O−O bond homolytic cleavage of the HHPP moiety and subsequent methyl radical release from the generated $(Me)_2C(OH)O\cdot$ intermediate.[25]

(34) Kinishita, A.; Ishimaru, H.; Nakashima, S.; Ogura, T.; Itoh, S. *J. Am. Chem. Soc.* **2008**, *130*, 4244–4245.